Proceedings of the ASME 2020
Dynamic Systems and Control Conference
DSCC2020
October 5-7, 2020, Virtual, Online

DSCC2020-3196

AN ULTRASOUND IMAGING BASED OBSERVER FOR ESTIMATING NMES-INDUCED MUSCLE FATIGUE: THEORY AND SIMULATION

Zhiyu Sheng[1], **Kang Kim**[1]*, **Nitin Sharma**[2]†
[1]University of Pittsburgh, Pittsburgh, PA, USA.
[2]North Carolina State University, Raleigh, NC and University of North Carolina at Chapel Hill, NC, USA.

ABSTRACT

Neuroprosthetic devices that use transcutaneous neuromuscular electrical stimulation (NMES) are potential interventions to restore skeletal muscle function in people with neurological disorders. As commonly noted, how to assess the NMES-induced muscle fatigue is a critical problem. This is because the capability of fatigue assessment is a necessary precursor for optimally modulating the NMES dosage to improve the control performance of a neuroprosthesis and ensure user's safety. To effectively estimate the NMES-induced muscle fatigue, this paper proposes a novel state observer that combines a mathematical predictive fatigue model and intermittent feedback from ultrasound-derived strain images. The strain images quantify muscle contractility during NMES. Principal component regression (PCR) is used to derive a relationship between the strain images and instantaneous muscle force production. Lyapunov stability analysis was performed to obtain the convergence property of the designed observer. A globally uniformly ultimately bounded (GUUB) result was obtained. Simulations based on pre-recorded data from a human experiment were also conducted to demonstrate the performance of the designed observer.

Key words: neuroprosthesis, neuromuscular electrical stimulation (NMES), muscle fatigue, ultrasound imaging, state observer, Lyapunov analysis

1 INTRODUCTION

Neurological injuries such as spinal cord injuries (SCI) and stroke cause mobility disorders and impair the quality of life of the affected persons. A recent estimate [1] shows that the annual incidence of SCI in the United States is about 54 cases per 1 million people. There are around 17,730 new SCI cases each year. In addition, approximately 7.0 million Americans (who are older than 20 years old) are self-reported to have had a stroke [2]. Research shows that neuroprosthetic devices that use neuromuscular electrical stimulation (NMES) can help restore or enhance the lost or impaired motor functions due to SCI or stroke [3]. Transcutaneous NMES applies external electrical pulses, via surface electrodes, to artificially activate a paralyzed or paretic skeletal muscle. NMES-elicited muscle contractions enable desired limb movements.

Modeling, design and control of NMES to restore limb functions is therefore of a great research interest. However, as commonly noted, NMES causes a rapid onset of muscle fatigue because the artificial muscle recruitment pattern is non-optimal compared to voluntary muscle contractions of a person with no neurological disorders [4]. Due to the NMES-induced muscle fatigue, the force generation capability of the muscle is quickly deteriorated. Thus, the onset of fatigue acts as a decreasing control gain in the feedback loop and degrades NMES control performance. The control error is likely to inflate if the control method is not robust or cannot adapt to the unknown time-variant fatigue state. In addition, excessively stimulating an already fatigued muscle may also result in injuries.

Therefore, for the purpose of ensuring both control performance and safety, estimating and monitoring the NMES-induced fatigue is important. To achieve this, multiple sensor modalities for direct fatigue assessment, for example, electromyography (EMG) or surface electromyography (sEMG), have been investigated in the literature [5]. Compared to other sensor modalities, ultrasound imaging has the advan-

*Co-contact author: Kang Kim {kangkim@upmc.edu}.
†Co-contact author: Nitin Sharma {nsharm23@ncsu.edu}.

tages such as non-invasiveness, capability to visualize muscle anatomy and a good signal-to-noise ratio for wide range of muscle depths. Our recent studies [6, 7] proposed high frame rate ultrasound strain images to characterize the fatigue effect. A potential correlation between the image-derived muscle strain and the force produced by muscle contraction was demonstrated. The strain-force correlation is promising to be further formulated as a measurement model to estimate the NMES-induced muscle fatigue. However, noise, artifacts and errors accumulated during the signal processing, as well as the unexplained variance that exists in the strain-force correlation, will likely affect the performance of fatigue estimation. In addition to those methodologies for direct fatigue assessment, mathematical models [8] use differential equations to predict the fatigue effect. These models do not work well by themselves due to difficulties of accurately identifying model parameters. More importantly, known initial conditions are essential to calculate the fatigue state based on differential equations, but in practice they are less likely available.

Despite the limitations of the mathematical predictive model, it provides a theoretical temporal trend of the fatigue development and is therefore useful to regularize the measurements from ultrasound images. In this paper, the proposed novel methodology for fatigue estimation combines a first order predictive fatigue model with measurements from ultrasound strain images and formulates a state observer. The predictive model provides a theoretical trend of the fatigue development, while the ultrasound measurements enable a fast convergence to the ground truth without knowing exact initial conditions. Despite the uncertainties that exist in both ultrasound imaging measurements and the predictive model, the observer, which works in a closed-loop structure, benefits the fatigue estimation in a way that the bias or errors of the estimation in the worst case can be bounded. Main challenges in the observer design of this problem are as follows. 1) Ultrasound measurements are only intermittently taken as feedback due to stability issues, as well as limitations of data acquisition and computational resources. 2) The stability of the observer needs to be guaranteed in the presence of model nonlinearities, uncertainties and measurement perturbations. Considering these challenges, a Lyapunov stability analysis was performed to prove a globally uniformly ultimate bounded (GUUB) convergence result of the designed observer. To demonstrate the proposed methodology, simulations were also conducted by using synthetic data generated from a preliminary experiment on human quadriceps muscle.

2 MATERIALS AND METHODS

2.1 Modeling and problem formulation

The muscle output force during NMES is determined by both muscle activation and fatigue status and is expressed as

$$F(t) = F_0 \mu(t) a(t), \tag{1}$$

where $t \in \mathbb{R}_{\geq 0}$ denotes the time vector, $F_0 \in \mathbb{R}$ is a constant that denotes the maximum force produced by the fully activated and completely non-fatigued muscle. $\mu \in [0,1]$ is the state variable for muscle fatigue. $a \in [0,1]$ is a time-variant parameter that describes the muscle activation. In this paper, to simplify the problem and to mainly focus on the estimation of the fatigue, isometric muscle contractions are assumed. Therefore, in Eqn. (1), force-length and force-velocity relationships, which typically appears in a Hill-Huxley model [9], are neglected.

To measure the force produced by each individual muscle group is a non-trivial problem. Therefore, we adopt a measurement model that is derived from the correlation between the force, F, and the synchronized 2-dimensional (2D) ultrasound strain images (See Section 2.4.) according to our recent study [7]. The correlation is between a 1D time series and a 2D matrix sequence (that consists of image pixels) and can therefore be identified by a principal component regression (PCR). As a result, it can be obtained that

$$F(t) = \hat{b} + \tilde{b} + (\hat{C}^T + \tilde{C}^T) S(t) + F_\delta(t), \tag{2}$$

where $S(t) \in \mathbb{R}^N$ is a column vector that contains all the N pixels in a strain image at time t. $\hat{C} \in \mathbb{R}^N$, $\hat{b} \in \mathbb{R}^N$ are coefficients identified by PCR to determine the strain-force correlation. $\tilde{b} \in \mathbb{R}^N$, $\tilde{C} \in \mathbb{R}^N$ and $F_\delta(t) \in \mathbb{R}^N$ are unknown perturbations to reflect the residues or unexplained variance during the regression. Denoting the sum of known or measurable quantities in Eqn. (2) as a measurement vector, $y(t) \in \mathbb{R}^N$, provides the measurement model as

$$y = \hat{b} + \hat{C}^T S(t) \tag{3}$$

The muscle activation, a, in Eqn. (1) can be written as

$$\begin{aligned} a(t) &= \hat{a}(t) + \tilde{a}(t) \\ &= a(0) e^{-w_a t} + w_a \int_0^t e^{-w_a (t-\tau)} u(\tau) d\tau + \tilde{a}, \end{aligned} \tag{4}$$

where $\hat{a} : \mathbb{R}_{\geq 0} \to [0,1]$ denotes the part that can be estimated by a nominal model of first order dynamics while $\tilde{a} \in [0,1]$ is the discrepancy between the estimated and the actual muscle activation. In Eqn. (4), $w_a \in \mathbb{R}_{>0}$ is the reciprocal of the time constant while $u : \mathbb{R}_{\geq 0} \to [0,1]$ represents the NMES input that is normalized by the maximum amplitude applied in the stimulation protocol. The state variable, μ, in Eqn. (1), describes the fatigue effect and can be further described by a first order differential equation [8] as

$$\dot{\mu} = w_f (\underline{\mu} - \mu) a + w_r (1 - \mu)(1 - a) + \mu_\delta. \tag{5}$$

In Eqn. (5), $w_f \in \mathbb{R}_{>0}$ and $w_r \in \mathbb{R}_{>0}$ are the reciprocal of the fatigue constant and the recovery constant, respectively. The constant, $\underline{\mu} \in [0,1]$, denotes the minimum that the fatigue

state, μ, can attain. The variable, $\mu_\delta \in [0,1]$, represents for the unmodeled uncertainties. The objective of the following sections is to design a state observer to estimate the fatigue state, μ, as defined in Eqn. (1) and Eqn. (5).

2.2 Observer design

The observer can be designed by superposing the nominal model of the fatigue state and the gain modulated feedback term from ultrasound imaging measurements. The nominal model can be derived, by replacing the variables in Eqn. (5) with known estimates, as

$$\dot{\hat{\mu}} = \hat{w}_f(\underline{\hat{\mu}} - \hat{\mu})\hat{a} + \hat{w}_r(1-\hat{\mu})(1-\hat{a}), \tag{6}$$

where the state variable, $\hat{\mu} \in [0,1]$, constants, $\hat{w}_f \in \mathbb{R}_{>0}$, $\underline{\hat{\mu}} \in [0,1]$ and $\hat{w}_r \in \mathbb{R}_{>0}$ are known estimates of μ, w_f, $\underline{\mu}$ and $\hat{w}_r$, respectively. The estimation error is defined as, $\tilde{\mu} = \mu - \hat{\mu}$, $\tilde{w}_f = w_f - \hat{w}_f$, $\underline{\tilde{\mu}} = \underline{\mu} - \underline{\hat{\mu}}$ and $\tilde{w}_r = w_r - \hat{w}_r$. The feedback term can be designed according to the ultrasound imaging based measurement model, given by Eqn (3). By combining Eqn. (6) and Eqn. (3), the observer to estimate the fatigue state is designed as

$$\dot{\hat{\mu}} = \hat{w}_f(\underline{\hat{\mu}} - \hat{\mu})\hat{a} + \hat{w}_r(1-\hat{\mu})(1-\hat{a}) + L_\sigma(y - \hat{a}\hat{\mu}F_0), \tag{7}$$

$$L_\sigma = \begin{cases} L & \sigma = 1 \\ 0 & \sigma = 0 \end{cases},$$

where $L_\sigma \in \mathbb{R}_{\geq 0}$ is a feedback gain. σ describes if the ultrasound image measurements are taken as the feedback ($\sigma = 1$) or not ($\sigma = 0$).

2.3 Stability analysis

The following theorem summarizes the convergent property of the designed observer in Eqn. (7).

Theorem 1. $\exists$ a finite $t^* \in \mathbb{R}_{>0}$, s.t., $\forall t \geq t^*$, the estimation error, $\tilde{\mu}(t) = \mu - \hat{\mu}$, satisfies $|\tilde{\mu}| \in \mathcal{L}_\infty$, if the feedback gain, L_σ is appropriately selected according to the subsequent analysis.

Proof. By using Eqn. (1), Eqn. (2) and Eqn. (3), as well as the relationship, $a = \hat{a} + \tilde{a}$, it can be obtained that

$$y = F_0\mu(\hat{a} + \tilde{a}) - \tilde{C}^T S(t) - \tilde{b} - F_\delta. \tag{8}$$

Further, using the definitions of $\tilde{w}_f$, $\underline{\tilde{\mu}}$ and $\tilde{w}_r$, as well as Eqn. (5), Eqn. (7) and Eqn. (8), $\dot{\mu} - \dot{\hat{\mu}}$ can be calculated algebraically as,

$$\begin{aligned}
\dot{\mu} - \dot{\hat{\mu}} =& (\hat{w}_f + \tilde{w}_f)(\underline{\mu} - \mu)(\hat{a} + \tilde{a}) + (\hat{w}_r + \tilde{w}_r)(1-\mu)(1-\hat{a}-\tilde{a}) \\
&+ \mu_\delta - \hat{w}_f(\underline{\hat{\mu}} - \hat{\mu})\hat{a} - \hat{w}_r(1-\hat{\mu})(1-\hat{a}) - L_\sigma(y - \hat{a}\hat{\mu}F_0) \\
=& -\tilde{\mu}(w_f a + w_r(1-a) + L_\sigma F_0(\hat{a} + \tilde{a})) \\
&+ (\hat{w}_f(\underline{\hat{\mu}} - \hat{\mu}) - \hat{w}_r(1-\hat{\mu}) - L_\sigma F_0\hat{\mu})\tilde{a} \\
&+ (\underline{\hat{\mu}} - \hat{\mu})\hat{a}\tilde{w}_f + \hat{w}_f\hat{a}\underline{\tilde{\mu}} + (1-\hat{\mu})(1-\hat{a})\tilde{w}_r \\
&+ (\underline{\hat{\mu}} - \hat{\mu})\tilde{w}_f\tilde{a} + \hat{w}_f\underline{\tilde{\mu}}\tilde{a} + \hat{a}\tilde{w}_f\underline{\tilde{\mu}} - (1-\hat{\mu})\tilde{w}_r\tilde{a} + \tilde{w}_f\underline{\tilde{\mu}}\tilde{a} \\
&+ \mu_\delta + L_\sigma(\tilde{C}^T S - \tilde{b} - F_\delta).
\end{aligned} \tag{9}$$

Design a Lyapunov functional candidate as

$$V = \frac{1}{2}\tilde{\mu}^2. \tag{10}$$

Using Eqn. (9), the time derivative of V along the trajectory of $\tilde{\mu}$ is derived and bounded as

$$\begin{aligned}
\dot{V} =& \tilde{\mu}(\dot{\mu} - \dot{\hat{\mu}}) \\
\leq& -(w_f a + w_r(1-a) + L_\sigma F_0\hat{a})\tilde{\mu}^2 + L_\sigma F_0 |\tilde{a}|\tilde{\mu}^2 \\
&+ \left|\hat{w}_f(\underline{\hat{\mu}} - \hat{\mu}) - \hat{w}_r(1-\hat{\mu})\right| |\tilde{a}| |\tilde{\mu}| + \left|(\underline{\hat{\mu}} - \hat{\mu})\hat{a}\right| \left|\tilde{w}_f\right| |\tilde{\mu}| \\
&+ \left|\hat{w}_f\hat{a}\right| \left|\underline{\tilde{\mu}}\right| |\tilde{\mu}| + |(1-\hat{\mu})(1-\hat{a})| |\tilde{w}_r| |\tilde{\mu}| \\
&+ \left|\underline{\hat{\mu}} - \hat{\mu}\right| \left|\tilde{w}_f\tilde{a}\right| |\tilde{\mu}| + \left|\hat{w}_f\right| \left|\underline{\tilde{\mu}}\tilde{a}\right| |\tilde{\mu}| + |\hat{a}| \left|\tilde{w}_f\underline{\tilde{\mu}}\right| |\tilde{\mu}| \\
&+ |1-\hat{\mu}| |\tilde{w}_r\tilde{a}| |\tilde{\mu}| + \left|\tilde{w}_f\underline{\tilde{\mu}}\tilde{a}\right| |\tilde{\mu}| + |\mu_\delta| |\tilde{\mu}| \\
&+ L_\sigma(\left|\tilde{C}^T S\right| + \left|\tilde{b} + F_\delta\right| - F_0\hat{\mu}|\tilde{a}|) |\tilde{\mu}|
\end{aligned} \tag{11}$$

For some constants, $\Psi_{\tilde{a}}$, $\Psi_{\tilde{w}_f}$, $\Psi_{\underline{\tilde{\mu}}}$, $\Psi_{\tilde{w}_r}$, $\Psi_{\tilde{w}_f\tilde{a}}$, $\Psi_{\underline{\tilde{\mu}}\tilde{a}}$, $\Psi_{\tilde{w}_f\underline{\tilde{\mu}}}$, $\Psi_{\tilde{w}_r\tilde{a}}$, $\Psi_{\tilde{w}_f\underline{\tilde{\mu}}\tilde{a}}$, Ψ_{μ_δ}, the corresponding quantities $L_i \in \mathbb{R}_{\geq 0}$, $i = 1, 2, ..., 10$, are defined as follows:

$$\begin{aligned}
L_1 &= \frac{\left|\hat{w}_f(\underline{\hat{\mu}} - \hat{\mu}) - \hat{w}_r(1-\hat{\mu})\right|^2 |\tilde{a}|^2}{4\Psi_{\tilde{a}}^2}, & L_2 &= \frac{\left|(\underline{\hat{\mu}} - \hat{\mu})\hat{a}\right|^2 \left|\tilde{w}_f\right|^2}{4\Psi_{\tilde{w}_f}^2}, \\
L_3 &= \frac{\left|\hat{w}_f\hat{a}\right|^2 \left|\underline{\tilde{\mu}}\right|^2}{4\Psi_{\underline{\tilde{\mu}}}^2}, & L_4 &= \frac{|(1-\hat{\mu})(1-\hat{a})|^2 |\tilde{w}_r|^2}{4\Psi_{\tilde{w}_r}^2}, \\
L_5 &= \frac{\left|\underline{\hat{\mu}} - \hat{\mu}\right|^2 \left|\tilde{w}_f\tilde{a}\right|^2}{4\Psi_{\tilde{w}_f\tilde{a}}^2}, & L_6 &= \frac{\left|\hat{w}_f\right|^2 \left|\underline{\tilde{\mu}}\tilde{a}\right|^2}{4\Psi_{\underline{\tilde{\mu}}\tilde{a}}^2}, \\
L_7 &= \frac{|\hat{a}|^2 \left|\tilde{w}_f\underline{\tilde{\mu}}\right|^2}{4\Psi_{\tilde{w}_f\underline{\tilde{\mu}}}^2}, & L_8 &= \frac{|1-\hat{\mu}|^2 |\tilde{w}_r\tilde{a}|^2}{4\Psi_{\tilde{w}_r\tilde{a}}^2}, \\
L_9 &= \frac{\left|\tilde{w}_f\underline{\tilde{\mu}}\tilde{a}\right|^2}{4\Psi_{\tilde{w}_f\underline{\tilde{\mu}}\tilde{a}}^2}, & L_{10} &= \frac{|\mu_\delta|^2}{4\Psi_{\mu_\delta}^2}.
\end{aligned} \tag{12}$$

Due to Eqn. (12), Eqn. (11) can be further bounded, after completing the squares, as the following

$$\begin{aligned}
\dot{V} \leq& -\tilde{\mu}^2(w_f a + w_r(1-a) + L_\sigma F_0\hat{a} - L_\sigma F_0 |\tilde{a}| - \sum_{i=1}^{10} L_i) \\
&+ \Psi^2 + L_\sigma(\left|\tilde{C}^T S\right| + \left|\tilde{b} + F_\delta\right| - F_0\hat{\mu}|\tilde{a}|) |\tilde{\mu}|,
\end{aligned} \tag{13}$$

$$\begin{aligned}
\Psi^2 =& \Psi_{\tilde{a}}^2 + \Psi_{\tilde{w}_f}^2 + \Psi_{\underline{\tilde{\mu}}}^2 + \Psi_{\tilde{w}_r}^2 + \Psi_{\tilde{w}_f\tilde{a}}^2 \\
&+ \Psi_{\underline{\tilde{\mu}}\tilde{a}}^2 + \Psi_{\tilde{w}_f\underline{\tilde{\mu}}}^2 + \Psi_{\tilde{w}_r\tilde{a}}^2 + \Psi_{\tilde{w}_f\underline{\tilde{\mu}}\tilde{a}}^2 + \Psi_{\mu_\delta}^2.
\end{aligned}$$

The following facts or assumptions need to be discussed before the stability results can be obtained:

F1) The Ψ^2 terms are used to facilitate the model uncertainties, $\tilde{w}_f$, $\tilde{w}_r$, etc. These constants proportionally determine the ultimate bound of the estimation error, $\tilde{\mu}$. Small Ψ^2 terms result in large L_i.

F2) The unknown model uncertainties, $\tilde{a}$, $\tilde{w}_f$, $\tilde{w}_r$, $\tilde{\underline{\mu}}$, μ_δ, are assumed bounded. Therefore, L_i terms can be bounded by known time dependent functions that can be calculated with the estimated constants or variables, $\hat{w}_f$, $\hat{w}_r$, $\hat{\underline{\mu}}$, $\hat{\mu}$, $\hat{a}$.

F3) The feedback gain, L, needs to be saturated by a constant, $\overline{L} \in \mathbb{R}_{>0}$, i.e., $\forall t$, $L \leq \overline{L}$.

F4) The value of $\sigma \in \{0,1\}$ is determined by if the inequality,

$$\overline{L}\,|\tilde{a}| + \frac{1}{F_0}\sum_{i=1}^{10} L_i \leq L\hat{a} \leq \overline{L}\hat{a}, \tag{14}$$

has a solution for L. $\sigma = 0$ if the solution set is empty while $\sigma = 1$ if the solution set is non-empty. In addition, the estimation of muscle activation, a, is assumed to be accurate enough so that $|\tilde{a}|$ can be bounded by a small number. Thus, the solution of Eqn. (14) always exists during some time period. In fact, in the situation when $|\tilde{a}|$ is large, the muscle activation, a, needs to be considered as a second unknown state for estimation. With a single measurement output, y, the observability is not well defined in the current problem formulation.

F5) The perturbations in the measurement model are bounded and it can be obtained that, for a constant, $M \in \mathbb{R}_{\geq 0}$,

$$(\left|\tilde{C}^T S\right| + \left|\tilde{b} + F_\delta\right| - F_0\hat{\mu}\,|\tilde{a}|)\,|\tilde{\mu}| \leq M\,|\tilde{\mu}|\,. \tag{15}$$

When F1, F2, ..., F5 are all satisfied, the following conclusions on stability can be obtained:

(i) $\sigma = 0$, $L_\sigma = 0$. Eqn. (13) becomes $\dot{V} \leq -\tilde{\mu}^2(w_f a + w_r(1-a) - \sum_{i=1}^{10} L_i) + \Psi^2$. It is obvious that $w_f a + w_r(1-a)$ can always be lower bounded by a positive constant. Therefore, there always exist a group of Ψ^2 terms such that $\sum_{i=1}^{10} L_i$ is small enough and $w_f a + w_r(1-a) - \sum_{i=1}^{10} L_i \geq \lambda_1$, where λ_1 is a positive constant. As a result,

$$\begin{aligned}\dot{V} &\leq -\tilde{\mu}^2\lambda_1 + \Psi^2 \\ &\leq -(1-\theta_1)\lambda_1\tilde{\mu}^2 - (\theta_1\lambda_1\tilde{\mu}^2 - \Psi^2),\end{aligned} \tag{16}$$

where θ_1 is a constant and $0 < \theta_1 < 1$. Therefore, $\forall |\tilde{\mu}| \geq \sqrt{\frac{\Psi^2}{\theta_1\lambda_1}}$, $\dot{V} \leq -(1-\theta_1)\lambda_1\tilde{\mu}^2$. According to [10], this implies that

$$|\tilde{\mu}| \leq \max\left\{|\tilde{\mu}(t_{1_0})|\,e^{-(1-\theta_1)\lambda_1(t_1 - t_{1_0})}, \sqrt{\frac{\Psi^2}{\theta_1\lambda_1}}\right\}, \tag{17}$$

where $t_1 \in \mathbb{R}_{\geq 0}$ denotes the time vector during this period while t_{1_0} is the initial time of this period.

(ii) $\sigma = 1$, $L_\sigma = L$. According to F4, $\exists\ \lambda_2 \in \mathbb{R}_{>0}$ as a constant, such that, $w_f a + w_r(1-a) + L_\sigma F_0\hat{a} - L_\sigma F_0\,|\tilde{a}| - \sum_{i=1}^{10} L_i \geq \lambda_2$. Further, according to F5, Eqn. (13) becomes

$$\begin{aligned}\dot{V} &\leq -\tilde{\mu}^2\lambda_2 + \Psi^2 + \overline{L}M\,|\tilde{\mu}|\,, \\ &\leq -(1-\theta_2)\lambda_2\tilde{\mu}^2 - (\theta_2\lambda_2\tilde{\mu}^2 - \overline{L}M\,|\tilde{\mu}| - \Psi^2),\end{aligned} \tag{18}$$

where θ_2 is a constant and $0 < \theta_2 < 1$. Similarly to (i), it can be obtained that, $\forall |\tilde{\mu}| \geq \frac{\overline{L}M + \sqrt{(\overline{L}M)^2 + 4\theta_2\lambda_2\Psi^2}}{2\theta_2\lambda_2}$, $\dot{V} \leq -(1-\theta_2)\lambda_2\tilde{\mu}^2$. Therefore,

$$|\tilde{\mu}| \leq \max\left\{|\tilde{\mu}(t_{2_0})|\,e^{-(1-\theta_2)\lambda_2(t_2 - t_{2_0})}, \frac{\overline{L}M + \sqrt{(\overline{L}M)^2 + 4\theta_2\lambda_2\Psi^2}}{2\theta_2\lambda_2}\right\}, \tag{19}$$

where $t_2 \in \mathbb{R}_{\geq 0}$ denotes the time vector during this period while t_{2_0} is the initial time of this period. Finally, since (i) and (ii) share a common Lyapunov functional, the error trajectory $|\tilde{\mu}|$ that is obtained by cascading (i) and (ii) in turn can be proven to be bounded as,

$$\begin{aligned}|\tilde{\mu}| &\leq \max\left\{|\tilde{\mu}(0)|\,e^{-\min\{(1-\theta_1)\lambda_1,(1-\theta_2)\lambda_2\}t}, \Omega\right\}, \\ \Omega &= \max\left\{\sqrt{\frac{\Psi^2}{\theta_1\lambda_1}}, \frac{\overline{L}M + \sqrt{(\overline{L}M)^2 + 4\theta_2\lambda_2\Psi^2}}{2\theta_2\lambda_2}\right\}.\end{aligned} \tag{20}$$

The GUUB convergence result is proven. It is noted that when the ultrasound imaging measurement is off ($\sigma = 0$), the observer is stable due to the convergence property of the nominal model Eqn. (6). However, the rate of convergence is small and the ultimate bound is determined by the model uncertainties. If the ultrasound imaging measurement can be frequently active, the rate of convergence is dominant by λ_2, which is determined and can be controlled by the feedback gain, L, selected according to Eqn. (14). The ultimate bound can also be controlled and minimized if the ultrasound imaging measurement kept active. In this situation, the fatigue estimation is dominant by direct ultrasound measurements and a saturation, $\overline{L}$, on the gain is required to control the estimation error due to measurement noise.

2.4 Synthetic data generation from a preliminary experiment

The preliminary experiment was conducted on a human participant with no neurological disorders. The participant was seated on a lab-built leg extension machine, as shown in Fig. 1a. The experimental protocols were approved by the Institutional Review Board (IRB) of the University of Pittsburgh. The NMES pulses (amplitude of 28 mA, pulse frequency of 35 Hz, pulse width of 300 μs) were generated from a stimulator (Rehastim 1, HASOMED GmbH,

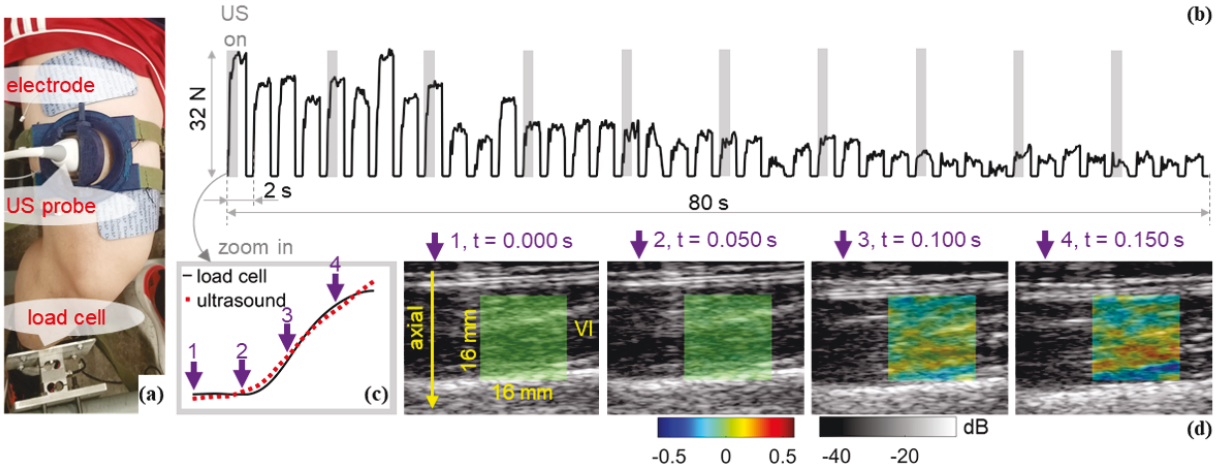

Figure 1. A preliminary experiment to generate the simulation data. (a) Experiment setup. Ultrasound images and force produced by muscle contractions were synchronously recorded through an ultrasound transducer and a load cell, respectively. NMES pulses were sent to stimulate the quadriceps muscle via two large electrode pads. (b) Load cell registered force produced by muscle contractions during the NMES protocol. Shadowed areas denote the time period when ultrasound imaging measurements are turned on. (c) Zoomed in force profiles during one muscle contraction. The solid line represents for the actual measured force by the load cell while the dotted line represents for the force derived from ultrasound strain images by PCR. (d) Co-registered and overlaid ultrasound B-mode images and the processed axial strain images using speckle tracking algorithm in a 16 by 16 mm region of interest on the vastus intermedius (VI) of the quadriceps muscle.

Germany) and activated contractions of quadriceps muscle through two electrodes (Dura-Stick Plus, 6.98 cm by 12.70 cm, Chattanooga, DJO, USA). Within 80 seconds, the stimulation was programmed to repeatedly turn on every 2 seconds with a duty cycle of 75%. The knee movement of the leg was constrained by a load cell (LC101-150, OMEGA Engineering, USA) that was attached normally to the front of the shank. The force produced by muscle contractions was registered at a sampling frequency of 1 kHz. A sequence of ultrasound images, which was synchronized to the force profile, was acquired using high frame rate planewave imaging (frame rate of 2kHz, center frequency of 5 MHz, sampling frequency of 20 MHz) with a ultrasound imaging research platform (Prodigy, S-Sharp, Taiwan). As shown by the shadowed area in Fig. 1b, the ultrasound measurements were only available for less than 1 second every 8 seconds. The instantaneous displacement vector field of the muscle was processed from the acquired ultrasound image sequence using a speckle tracking algorithm [11]. The strain images were then obtained by taking spatial gradient of the displacement vector field along the axial direction, as shown by the overlaid and co-registered ultrasound images in Fig. 1d. Estimated force profiles were calculated using the strain images according to Eqn. (3) with identified regression coefficients. Fig. 1c shows a comparison between the image-derived force profile and the actual force data registered by the load cell.

The actual force data was used to generate the ground truth of the fatigue state in simulation. According to Eqn. (1), the fatigue state, μ, can be considered as the normalized force and was calculated by $\mu = F/(F_0 a)$, where F is the recorded force and F_0 is the initial force peak. The muscle activation, a, was computed using Eqn. (4). By neglecting the fatigue effect during the first several muscle contractions,

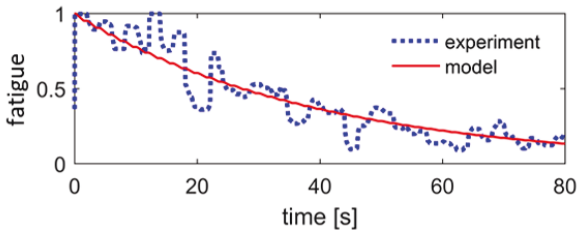

Figure 2. Curves of the fatigue state. The dotted line was obtained by normalizing the force profile recorded from the experiment. The solid line was generated by the fatigue model with the identified model parameters (See text.). The solid line was used as the ground truth during simulations.

the activation parameter, w_a, can be identified by fitting the recorded force profile to a first order step response, provided the NMES input is a constant step during one muscle contraction. $\tilde{a}$ is ignored in the simulation. As a result, the curve representing for the actual fatigue state, μ, recorded from the experiment is obtained, as shown by the dotted line in Fig. 2. After numerically integrating both sides of Eqn. (5) (and ignoring μ_δ), the resultant equation,

$$\mu = \mu(0) + w_f \underline{\mu} \int_0^t a dt + w_f \int_0^t (-\mu a) dt + w_r \int_0^t (1 - \mu - a + \mu a) dt, \quad (21)$$

is a multi-variate linear relationship among μ, $\int_0^t a dt$, $\int_0^t (-\mu a) dt$ and $\int_0^t (1 - \mu - a + \mu a) dt$. By applying a constrained multi-variate linear regression on Eqn. (21), parameters, $\underline{\mu}$, w_f and w_r can be obtained. The results were summa-

w_a [s^{-1}]	$\underline{\mu}$	w_f[s^{-1}]	w_r[s^{-1}]
4.47	3.80e-9	3.95e–2	4.07e-10

Table 1. Identified parameters of the muscle activation (Eqn. (4)) and the fatigue model (Eqn. (5)).

rized in Tab. 1. Finally, as shown by the solid line in Fig. 2, a synthetic fatigue curve was generated using Eqn. (5) with the identified model parameters. This curve was used as a ground truth for fatigue estimation during the simulation.

3 RESULTS AND DISCUSSION

Simulation was performed to estimate the state variable of NMES-induced muscle fatigue by using the designed observer in Eqn. (7). Figure 3 summarizes the results. In Fig. 3a, the ground truth was intentionally generated with $\mu(0) = 0.67$ while the observer that is blind to this initial condition was initialized with a random guess, $\hat{\mu}(0) = 1$. The feedback gain when ultrasound imaging measurements were available was selected as $L = 0.08$. By comparing the dotted line and the solid line, it is seen that the estimated fatigue state converged to the ground truth despite the initial discrepancy. Particularly, during the time period when the ultrasound imaging was active, the rate of convergence, shown as the negative slope of the solid curve, was greatly increased, compared to the relatively flat period (when the estimation was dominant by the nominal model). Therefore, it was demonstrated that the ultrasound feedback can accelerate the convergence of estimation. This will be crucial for the proposed methodology when adopted in neuroprosthetic devices so that the controlled modulation of the NMES input can response in time.

Figure 3b compares the estimated force curve (calculated by Eqn. (1) with the observed fatigue state) with the simulated ground truth. Figure 3c shows the fatigue estimation when L is chosen as different values. It demonstrates that an increased gain makes the ultrasound feedback more dominant in the fatigue estimation. As a result, the initial transient time period (before the estimated state converges to its ultimate bound) is much shorter. The estimation error within this period is also smaller. However, with an increased contribution from the ultrasound measurement, the observer also attained a curve that is mostly determined by the image-derived force profile. In this simulation, because the residues in the PCR (when calculating y in the feedback term of Eqn. (7)) can be inherited and inflate the *LM* term (as in Eqn. (15)) when L is large, an estimation bias from the ground truth can be expected, as shown by the solid curves (gain = 0.2, 0.4). As shown in Tab. 2, the root mean square error (RMSE), which is between the observer estimated force and the ground truth and is calculated in different time intervals, can demonstrate the discussion in this paragraph.

To test the robustness of the observer to model uncertainties, $\tilde{w}_f$, $\tilde{w}_r$ and $\tilde{\underline{\mu}}$, synthetic perturbations that follows zero mean Gaussian distributions were added to the corresponding model parameters. The situations when the feedback gain were chosen as, 0.08 and 0.2, respectively, and the variance of the Gaussian distribution was chosen as, 0.1%, 0.5%, 1%, 2%, 5%, 10% and 20%, respectively, of the unperturbed parameter, were simulated for 10000 independent realizations. The results are summarized by Tab. 3 in the form of mean $\pm$ standard deviation of the RMSE. Overall, the observer showed a good robustness in the simulation and a larger gain (0.2) can potentially yield better robustness than a smaller gain (0.08).

gain	**0**	**0.05**	**0.08**	**0.2**	**0.4**
$t \in [0,64]$	3.68	2.66	2.34	2.00	2.09
$t \in [10,64]$	3.07	1.74	1.30	1.17	1.64
$t \in [20,64]$	2.58	1.04	0.56	1.10	1.67
$t \in [30,64]$	2.19	0.61	0.19	1.08	1.38
$t \in [40,64]$	1.88	0.41	0.15	0.77	0.83

Table 2. RMSE between the ground truth and the observer estimated force (N) under different feedback gains calculated in different time (s) intervals.

perturbation	$L = 0.08$	$L = 0.2$
0.1%	2.34 ± 0.00	2.00 ± 0.00
0.5%	2.34 ± 0.01	2.00 ± 0.00
1%	2.34 ± 0.02	2.00 ± 0.00
2%	2.34 ± 0.03	2.00 ± 0.00
5%	2.35 ± 0.08	2.00 ± 0.01
10%	2.35 ± 0.16	2.01 ± 0.02
20%	2.40 ± 0.28	2.04 ± 0.09

Table 3. Mean $\pm$ standard deviation of the RMSE obtained in a 10000-realization simulation when different perturbations (See text.) were added to the model parameters.

4 CONCLUSION

This paper proposed an ultrasound imaging based observer to estimate the NMES-induced muscle fatigue. The observer consists of a nominal fatigue model of first order dynamics and an intermittently active feedback term from ultrasound imaging measurements. The stability of the observer was thoroughly analyzed through a Lyapunov analysis to obtain the GUUB convergence result. To further demonstrate the property and feasibility of the observer, simulations were performed using synthetic data generated from an experiment on the human quadriceps muscle. The simulations show that the designed observer is promising to estimate effects of the NMES-induced muscle fatigue. The simulations also provide a general guideline, which is consistent with the theoretical analysis, for tuning the feedback gain.

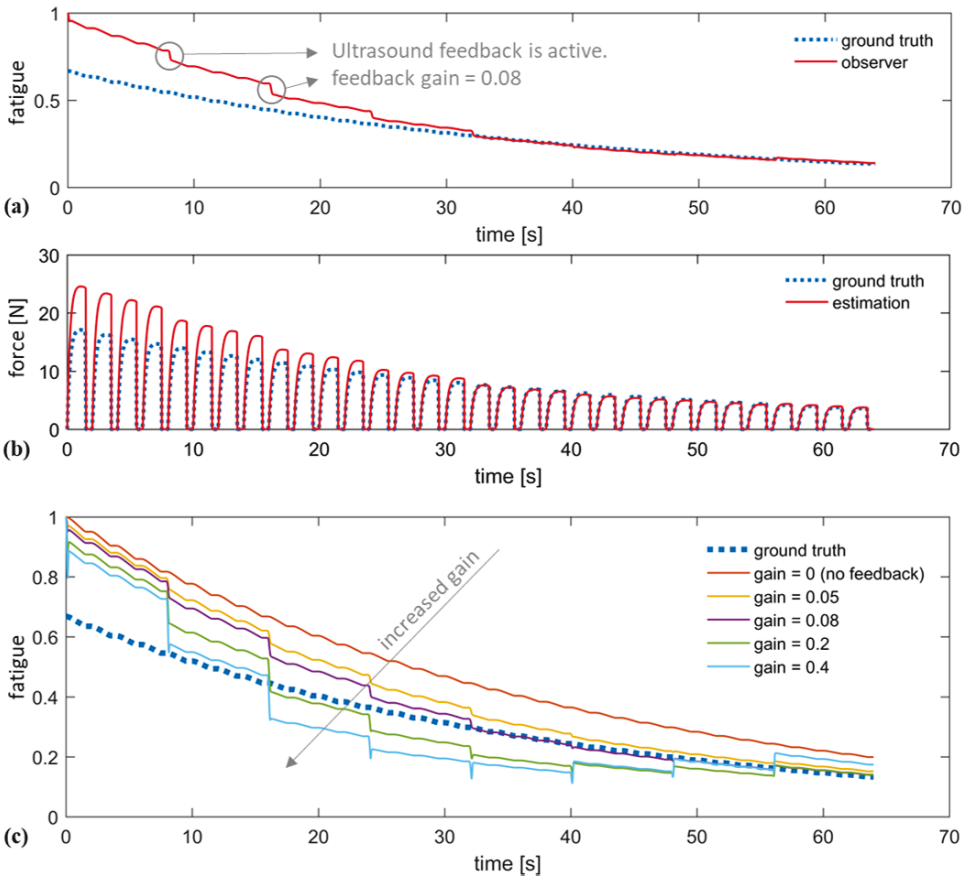

Figure 3. Simulation results of fatigue estimation using the designed observer. (a) The observed fatigue state when the feedback was 0.08, compared with the ground truth. (b) Estimated force profile using the estimated fatigue state from (a), compared with the ground truth. (c) Curves of estimated fatigue state using different feedback gains, compared with the ground truth.

Acknowledgements

This research is supported by NSF award number: 1646009. This research is supported in part by the University of Pittsburgh Center for Research Computing through the resources provided.

References

[1] "National Spinal Cord Injury Statistical Center. Facts and Figures at a Glance." *Birmingham, AL: University of Alabama at Birmingham* (2016): pp. 1–2.

[2] Benjamin, Emelia J, Virani, Salim S, Callaway, Clifton W et al. "Heart disease and stroke statistics2018 update: a report from the American Heart Association." *Circulation* .

[3] Lynch, C. L. and Popovic, M. R. "Functional electrical stimulation." *IEEE Control Syst. Mag.* Vol. 28, No. 2 (2008): pp. 40–50.

[4] Bickel, C Scott, Gregory, Chris M and Dean, Jesse C. "Motor unit recruitment during neuromuscular electrical stimulation: a critical appraisal." *Eur. J. Appl. Physiol.* Vol. 111, No. 10 (2011): pp. 2399–2407.

[5] Al-Mulla, Mohamed R, Sepulveda, Francisco and Colley, Martin. "A review of non-invasive techniques to detect and predict localised muscle fatigue." *Sensors* Vol. 11, No. 4 (2011): pp. 3545–3594.

[6] Sheng, Z., Sharma, N. and Kim, K. "Quantitative assessment of changes in muscle contractility due to fatigue during NMES: an ultrasound imaging approach." *IEEE Trans. Biomed. Eng.* Vol. 67 (2019): pp. 832–841.

[7] Sheng, Z., Sharma, N. and Kim, K. "Ultra-High-Frame-Rate Ultrasound Monitoring of Muscle Contractility Changes Due to Neuromuscular Electrical Stimulation." *Ann. Biomed. Eng., https://doi.org/10.1007/s10439-020-02536-7* .

[8] Riener, R., Quintern, J. and Schmidt, G. "Biomechanical model of the human knee evaluated by neuromuscular stimulation." *J. Biomech.* Vol. 29 (1996): pp. 1157–1167.

[9] Winter, D. *Biomechanics and motor control of human movement*. Wiley (2009).

[10] Khalil, H. *Nonlinear Systems*, 3rd ed. Prentice Hall (2002).

[11] Lubinski, Mark A, Emelianov, Stanislav Y and O'Donnell, Matthew. "Speckle tracking methods for ultrasonic elasticity imaging using short-time correlation." *IEEE Trans. Ultrason. Ferroelectr. Freq. Control* Vol. 46, No. 1 (1999): pp. 82–96.